Tribological and mechanical performance evaluation of metal prosthesis components manufactured via metal injection molding

Virginia Melli · Mateusz Juszczyk · Enrico Sandrini · Giovanni Bolelli · Benedetta Bonferroni · Luca Lusvarghi · Alberto Cigada · Tiziano Manfredini · Luigi De Nardo

Received: 8 May 2014 / Accepted: 23 July 2014 / Published online: 11 January 2015

1 Introduction

The figures for total joint arthroplasty (TJA) show a stable trend of growth in several Countries [1, 2], being correlated to an increase of life expectation and quality of life standards [3]. Such class of surgeries, together with the social and clinical impact, strongly burden the healthcare system costs. As pointed out by Barber and Healy [4], attempts to reduce prosthetic costs should be very effective in reducing the overall costs of performing TJA for it represents the highest percentage cost item. Several efforts have been focused on new manufacturing technologies with lower production costs, in order to replace conventional technologies for TJA components made via casting or forging [5–7].

Metal Injection Molding (MIM) technology can provide quasi-net shape to raw materials, avoiding the machining step and saving resources up to about 20–50 % of the final cost [7]. In order to adjust the material properties to standard require-ments (ISO 5234-4; ASTM F75) the process was optimized in the last years through the evaluation of the effects of alloy composition, sintering temperature, thermal treatment and hot isostatic pressing on hardness, wear behavior and tensile properties of the MIM CoCrMo products [8–11]. A strict regulation (ASTM F2083/ISO 21536), requiring same prop-erties and behavior of the commercialized component at least

V. Melli · A. Cigada · L. De Nardo
Department of Chemistry, Materials, and Chemical Engineering "G. Natta", Politecnico Di Milano, Piazza L. Da Vinci 32, 20133 Milan, Italy

M. Juszczyk · E. Sandrini
Nanosurfaces Industries, Via Buozzi 13/15, Granarolo Emilia 40057, Bologna, Italy

G. Bolelli · B. Bonferroni · L. Lusvarghi · T. Manfredini
Department of Engineering "Enzo Ferrari", Università Di Modena E Reggio Emilia, Via P. Vivarelli 10/1, 41125 Modena (MO), Italy

A. Cigada · L. De Nardo (✉)
Local Unit INSTM – Consorzio Interuniversitario Nazionale Per La Scienza E La Tecnologia Dei Materiali, Florence, Italy
e-mail: luigi.denardo@polimi.it

from the biocompatibility, fatigue and electrochemical point of view, is foreseen for implantable devices. Recently, it has been shown that CoCrMo medical grade alloys processed via MIM have acceptable electrochemical resistance and in vitro biocompatibility [12].

An important aspect to be considered for the production of MIM tibial tray is its fatigue performance. Indeed, failure of tibial trays due to fatigue fracture has been reported in patients and efforts in order to evaluate a fatigue threshold limit for this device have been carried out [13, 14]. Loss of bony support, due to stress shielding bone remodeling, osteolysis, severe varus or valgus deformities, poor fixation or axial malalignment, is the main cause affecting the fatigue performance, as it results in overloading of the component. The design and the manufacturing process are the crucial parameters influencing the tibial tray fatigue limit [13–16].

The aim of this work is to validate the MIM technology by comparing microstructure, materials intrinsic mechanical properties, and fatigue resistance of the obtained components with analogues, produced via conventional manufacturing processes.

2 Materials and methods

2.1 Materials preparation

CoCrMo (ISO 5832-4) disks ($\Phi = 20$ mm, thick-ness $= 5$ mm) were prepared by metal injection molding (MIM) and investment casting (CAS). CAS disks were used as negative control material versus MIM for the evaluations of microstructure and mechanical properties. The chemical compositions of both kinds of samples are reported in Table 1. They were assessed by X-ray fluo-rescence (NITON XLt 999 VW, Thermo Fisher Scientific, Munich, Germany) and the amount of carbon was deter-mined by a combustion method using a Leco CS 230 C analyzer (Leco Corporation, St. Joseph, MI, USA).

CAS specimens were provided by SAMO SpA (Granarolo Emilia, Bologna, Itay) while MIM specimens, produced according to the process described in ref [9–11], were provided by Mimest (Pergine Valsugana, Trento, Italy).

Table 1 Alloys' elemental composition (in weight percentage) of CAS and MIM specimens used in the microstructural characterization and of the corresponding complete tibial trays (TT-CAS and TT-MIM)

	Cr	Mo	Ni	Fe	C	Mn	Si	Co
$\%_{wt}$ CAS	28.6	5.46	0.12	0.4	0.25	0.54	0.72	Bal
$\%_{wt}$ MIM	28.0	6.1	0.16	0.22	0.24	0.67	0.56	Bal
$\%_{wt}$ TT-CAS	29.0	6.22	–	0.85	0.24	0.37	–	Bal
$\%_{wt}$ TT-MIM	28.3	6.13	–	0.51	0.22	0.76	–	Bal

Tibial trays of the most critical size, previously determined through FEM simulation of the load configuration foreseen in the fatigue test, were provided of the MIM type (TT-MIM), supplied again by Mimest, and of the cast type (TT-CAS), supplied by SAMO SpA. Tested tibial trays design is of non-constrained type, following the ASTM F2083 classification, and they were provided in the final product condition just before sterilization and packaging. The chemical composition of the tibial trays, measured in the same way as described above, is reported in Table 1.

2.2 Mechanical characterization

Hardness and elastic modulus were assessed by depth-sensing Vickers micro-indentation testing (Micro-Combi Tester, CSM Instruments, Peseux, Switzerland) according to the Oliver-Pharr method [17], in compliance with the ISO 14577 standard. A total of 20 indentations were performed on each kind of sample, with a maximum applied load of 3 N, loading and unloading rates of 2.4 N min^{-1} and holding time of 15 s at maximum load. The Poisson's ratio of the material was assumed to be 0.30.

Scratch tests (Micro-Combi Tester) were performed on the polished surfaces of the disk samples using a Rockwell C-type conical diamond indenter with 200 μm-radius spherical tip. The tests involved the application of a constant load of 10 N over a scratch length of 4 mm, with scratch speed of 1 mm min^{-1}. The complete 3-D profile of the scratch track was acquired by optical confocal profilometry (Conscan profilometer, CSM Instruments) and the ratio between the volume of the material piled up along the sides of the central groove (V_P) and the volume of the groove itself (V_G) was computed (Fig. 1).

Rotating unidirectional sliding wear tests were performed in ball-on-disk configuration using a pin-on-disk tribometer (High Temperature Tribometer, CSM Instruments) equipped with spherical sintered alumina pins (nominal hardness 19 GPa) of 6 mm diameter pressed against rotating polished disk samples. The wear track radius was 3.5 mm; the disk revolution speed 150 rpm; a total number of 50,000 revolutions were performed. Dry sliding wear tests were carried out at room temperature ($T = (25 \pm 2)$ °C, (58 ± 2) % relative humidity) with normal loads of 3 N and 5 N. Additional tests were performed under a normal load of 5 N with the samples immersed in 50 mL of a simulated body fluid (SBF) solution prepared according to Kokubo et al. [18] and consisting of 7.909 g L^{-1} NaCl, 0.353 g L^{-1} $NaHCO_3$, 0.042 g L^{-1} KCl, 0.311 g L^{-1} $MgCl_2$, 0.367 g L^{-1} $CaCl_2$, 0.071 g L^{-1} Na_2SO_4, 6.057 g L^{-1} tris-(hydroxy-methyl) aminomethane (TRIS), 0.268 g L^{-1} Na_2HPO_4, with pH adjusted to 7.4 by additions of HCl 1 M. This solution simulates the inorganic part of human plasma [18].

The wear volume of the samples was assessed by optical confocal profilometry (Conscan) and converted to wear

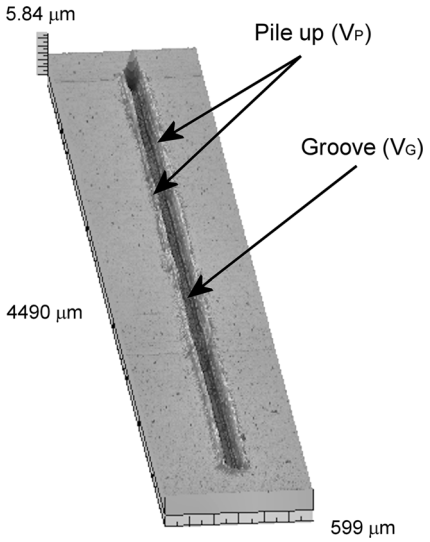

Fig. 1 Topography of a scratch track with indication of the lateral pile-up volume V_P and of the central groove volume V_G

rate (volume loss per unit sliding distance and unit normal load). The wear scar produced on the samples was further inspected by optical microscopy and SEM (XL30, FEI). The wear debris collected on the samples after testing in dry conditions was inspected by environmental scanning electron microscopy (ESEM: Quanta 200, FEI) + energy dispersive X-ray microanalysis (EDX: INCA, Oxford Instruments Analytical, High Wycombe, UK) under low vacuum conditions ($\approx$1 mbar water vapor atmosphere).

2.3 Device fatigue performance

To detect the fatigue limit of the final device and compare the TT-MIM and TT-CAS performances, the equation proposed by Dixon was applied:

$$P_{D(50\%)} = P_f + K \cdot d \quad (1)$$

where $P_{D(50\ \%)}$ is the fatigue limit, as the load associated with the 50 % failure probability, P_f is the last value of the load sequence and d is the load step required by the staircase fatigue loading protocol and K is a statistical coefficient tabulated in [19].

Six tibial trays per each type were tested on axial servohydraulic testing machine (Federico Giuliani, Forlì, Italy) equipped with close-loop digital controller RT3 V.3.3 (Trio Sistemi e Misure S.r.l., Dalmine BG, Italia). Testing setup is described in ASTM F1800-07 and ISO 14789-1:2000 and shown in Fig. 2. TT were rigidly fixed through PMMA bone cement to a specimen holder clamped to the machine piston. Load was applied on a defined circular area with an UHMWPE insert. Loads were measured with a 25 kN load cell (HBM, Darmstadt, Ger-many). The loading application point was chosen in the most critical position for stresses on tibial trays following indications provided by a FEM simulation, performed by the technical department of SAMO Spa, in the load con-figuration foreseen for the fatigue test. The loading appli-cation point chosen was in a non-physiological situation, at the maximum rollback of the knee, in order to obtain conservative results.

Sinusoidal load was applied to each specimen with a maximum to minimum ratio of 10 and frequency of 10 Hz for 5 millions cycles. Starting mean load and load step were set on the basis of previous experience on tibial trays fatigue test; 1,320 N and 1,750 N were selected as starting loads for TT-MIM and TT-CAS respectively, with a load step of 50 N.

Observations of fracture surfaces after the test were performed by stereo microscopy (WILD 6×–50× and digital camera LEICA DFC290, Solms, Germany).

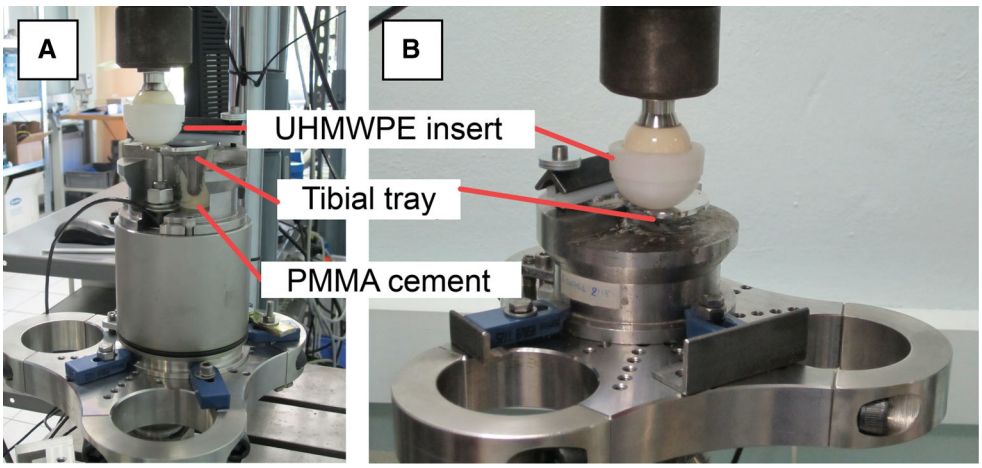

Fig. 2 Device fatigue testing setup. **a** Configuration with LVDT for static test; **b** configuration for cyclic test as prescribed by ISO and ASTM standards

Table 2 Results of depth-sensing Vickers micro-indentation tests and of scratch tests on cast and MIM CoCrMo alloy samples

	MIM	CAS
HV_{3N}	335 ± 12	514 ± 16
E (GPa)	278 ± 31	281 ± 8
V_G (μm^3)	(8.27 ± 0.19) × 10^5	(3.15 ± 0.36) × 10^5
V_P/V_G	0.72 ± 0.02	0.96 ± 0.04

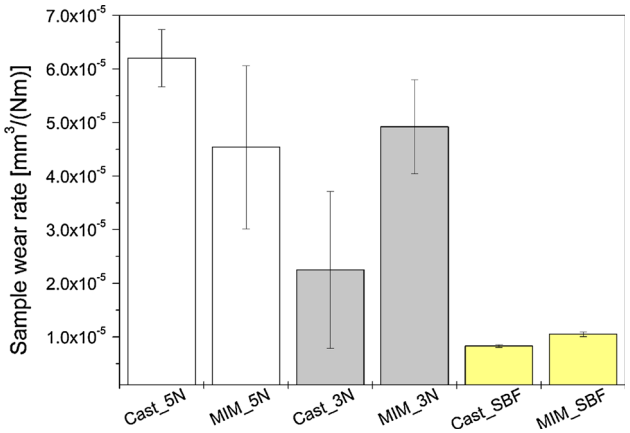

Fig. 3 Wear rates after ball-on-disk sliding wear tests in dry conditions with 3 and 5 N normal loads, and in wet condition (immersion in SBF solution) with 5 N normal load

An additional static load test was performed in the same configuration, with a displacement rate of 0.1 mm s^{-1}, to obtain the load–displacement curve and the yield limit of the tray. To measure actual displacement, an LVDT GPA-750-050 (Macrosensors, Pennsauken NJ, USA) was used in contact with the tibial tray under surface, in line with the load application axis.

3 Results

3.1 Micromechanical and tribological characterization

The results of micromechanical and tribological characterization are summarized in Table 2.

CAS specimens exhibit larger Vickers microhardness when compared to MIM specimens while the elastic moduli do not differ.

Scratch tests indicate that, compared to MIM, CAS specimens develop smaller grooves (lower V_G) with larger V_P/V_G ratio between pile-up volume and groove volume.

Dry sliding wear tests carried out under a 3 N normal load (Fig. 3) indicate an improved wear resistance of CAS samples over MIM ones. Upon increasing the normal load to 5 N, however, the wear rate of the CAS sample becomes somewhat larger than that of the MIM

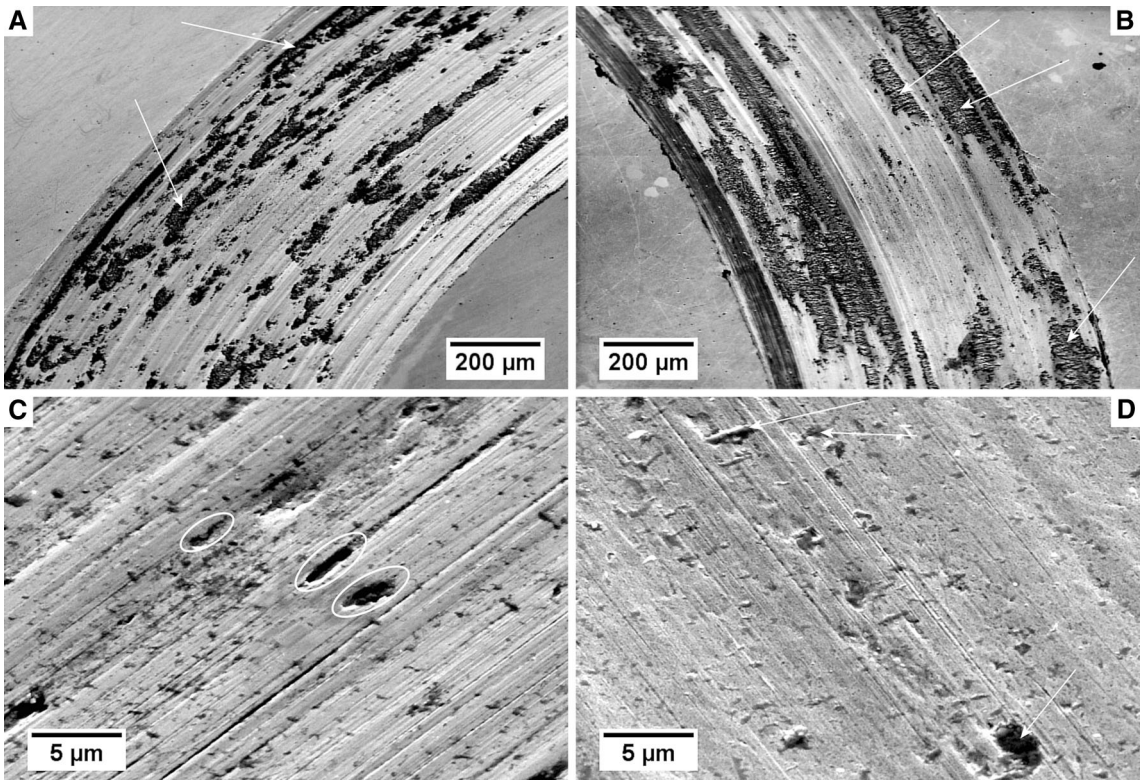

Fig. 4 SEM micrographs (secondary electrons) of the wear scars produced on a cast (**a**, **c**) and MIM (**b**, **d**) sample after dry ball-on-disk wear testing with 5 N normal load. *Arrows* indicate some of the visible oxide clusters; *circles* in panel (**c**) indicate pull-outs

one, although, in all of the dry sliding wear tests, sig-nificant experimental scatter in wear rate data is found (as indicated by the large standard deviations, plotted as error bars in Fig. 3).

Observation of the wear scars produced in dry conditions (under both normal loads) indicates that wear mainly proceeds by abrasive grooving, as expected (Fig. 4a, b). Tribo-oxidation mechanisms are, however, also active, which is witnessed by the presence of oxide clusters smeared and flattened onto the sample surfaces (Fig. 4, see arrows). The fine, rounded (Fig. 5a, b), oxi-dised (Fig. 5c) debris particles collected outside the wear scars are also consistent with the typical morphology of tribo-oxidative wear debris. Fine metal fragments removed by abrasive grooving are indeed easily oxidised (due to their small size and to the large flash temperature [20] which they may attain when they are developed). The oxide particles trapped within the wear scar are further broken down to micrometric fines (as seen in Fig. 5a), and some of them can be smeared onto the wear scar itself, leading to the formation of the men-tioned oxide clusters.

Clusters are repeatedly formed and detached during the wear test: fragments of flattened clusters, detached from the wear track surface, are indeed recognizable inside the wear debris as large, platelet-like oxidized flakes (Fig. 5a, b: see arrows and circled area). Such continuous formation and detachment of oxide clusters causes instability of the contact conditions, resulting in large fluctuations of the friction coefficient (Fig. 6). This phenomenon is probably responsible for the large experimental scatter in the wear rate values as well.

As the load is increased to 5 N, wear mechanisms do not change significantly; however, small pits appear on the surface of the CAS samples (Fig. 4c, circled areas), conversely not found on the MIM sample (Fig. 4 d: only dark oxide clusters are seen in this micrograph).

When samples are completely immersed in the SBF solution during the ball-on-disk test, wear rates are significantly decreased (Fig. 3) and contact conditions become stable, as shown by the friction curves in Fig. 6. The liquid indeed lessens flash heating of the mating sur-faces and of debris particles, preventing oxidation phe-nomena (Fig. 7). Moreover, although the SBF solution cannot be compared to an oil lubricant in its load carrying capability, it can partly mediate the contact between the sample and the Al_2O_3 spherical counterpart. For both MIM and cast samples wear rates in wet conditions are below 1×10^{-5} mm^3 N^{-1}m^{-1}, witnessing to satisfactory sliding wear properties in liquid-mediated contacts for both kinds of materials.

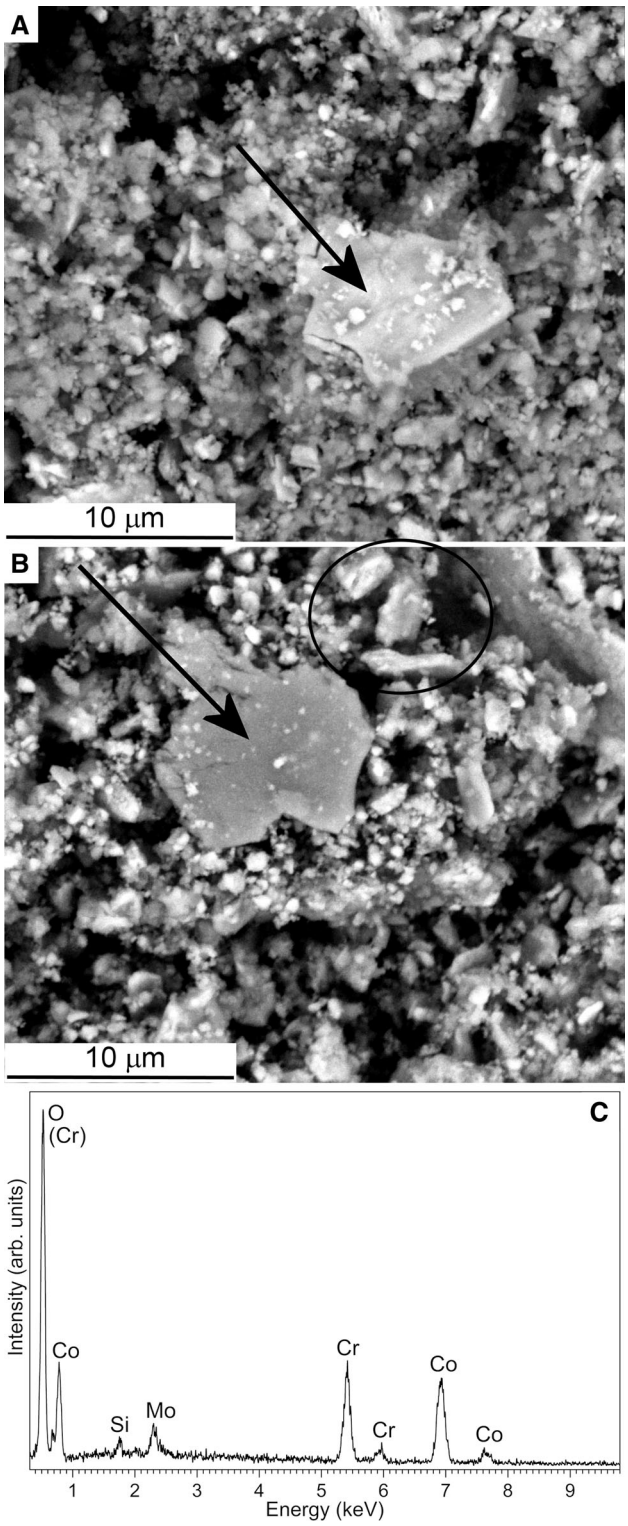

Fig. 5 ESEM micrographs (secondary electrons) of the wear debris collected on the cast (**a**) and MIM (**b**) samples after dry ball-on-disk wear testing with 5 N normal load, and representative EDX micrograph of the debris (**c**). *Arrows* and *circles* indicate larger, platelet-like debris particles

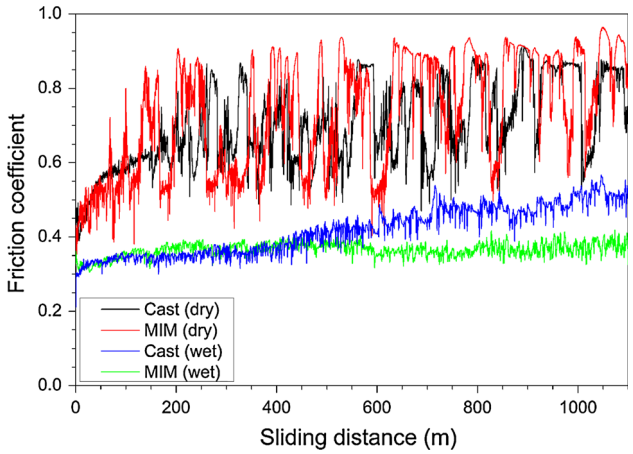

Fig. 6 Friction curves recorded during dry and wet (SBF immersion) sliding wear testing of cast and MIM samples with 5 N normal load

3.2 Device fatigue performance

In Fig. 8 the load–displacement curves and the tested TT-MIM and TT-CAS specimens are reported. The static mechanical behavior observed is equal for the two kind of TT but some peculiarities could be observed from the deformed surfaces. The TT region subdued to plastic deformation lost its original light reflectance in two different ways: TT-MIM showed a fine rough opaque surface while TT-CAS maintained a shinier appearance, as if the plastic flux followed macroscopic preferential planes.

In Tables 3 and 4 the loading sequence obtained is reported for TT-MIM and TT-CAS respectively. From these results the fatigue limit for 5 millions cycles life was calculated using Dixon's equation and statistical coefficients. [19] TT-MIM showed a fatigue limit of (1,625 ± 44) N and TT-CAS showed a fatigue limit of (1,766 ± 52) N. Crack initiation and propagation were analogue for TT-CAS and TT-MIM, in Fig. 9 an example of TT rupture is reported. Failure started from the top surface of the TT from the posterior intercondylar boundary with an average crack propagation oblique through the free condyle surface. Except in one case, crack propagated through the whole tray thickness with a 45 deg orientation, indicating presence of torque in that zone.

In Fig. 10 the fracture surfaces of TT-MIM and TT-CAS that failed the fatigue test are reported. The crack propagation path was visually followed during the loading cycles highlighting its starting from the upper part of the tray and growth through the thickness. The two fracture morphologies appeared rather different. TT-CAS fracture surface is smoother than the TT-MIM one and shows the lines of crack propagation, typical of fatigue fracture. Differently, TT-MIM fracture surface has a rough topography that suggests a more brittle behavior.

4 Discussions

4.1 Micromechanical and tribological characterization

From a previous microstructure study of CAS and MIM CoCrMo alloy [12] some differences in the metal grain structure were pointed out. As reported in that study, the CAS alloy possesses a dendritic microstructure, with finer grain size, and contains a large amount of precipitated carbides. On the other hand, the MIM sample features coarser polygonal crystals with numerous stacking faults; it possesses almost no carbide precipitates, but exhibits a distributed fine porosity [12].

The higher Vickers hardness of the CAS specimen is therefore consistent with the previously observed finer grain size and, particularly, with the presence of a larger

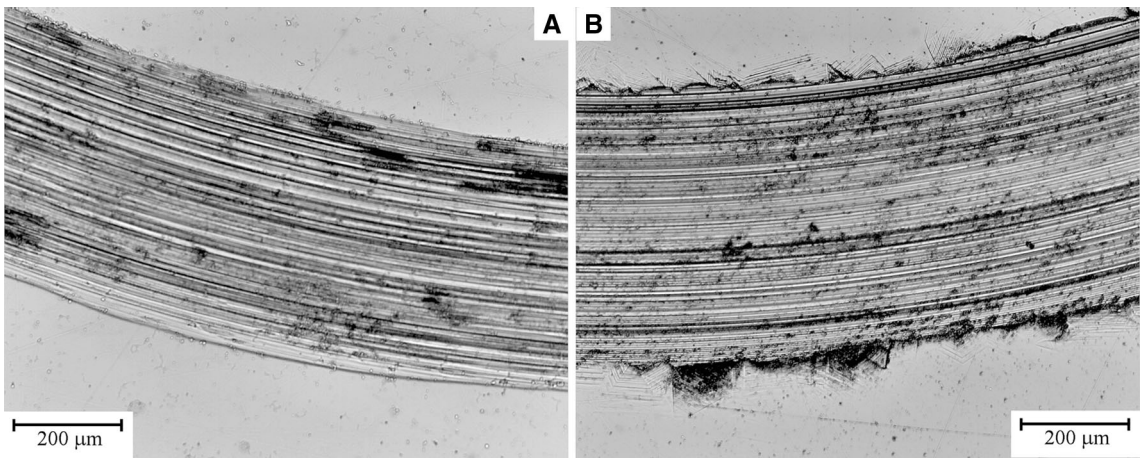

Fig. 7 Optical micrographs of the wear scars produced on cast (**a**) and MIM (**b**) samples after wet (SBF immersion) ball-on-disk sliding wear testing

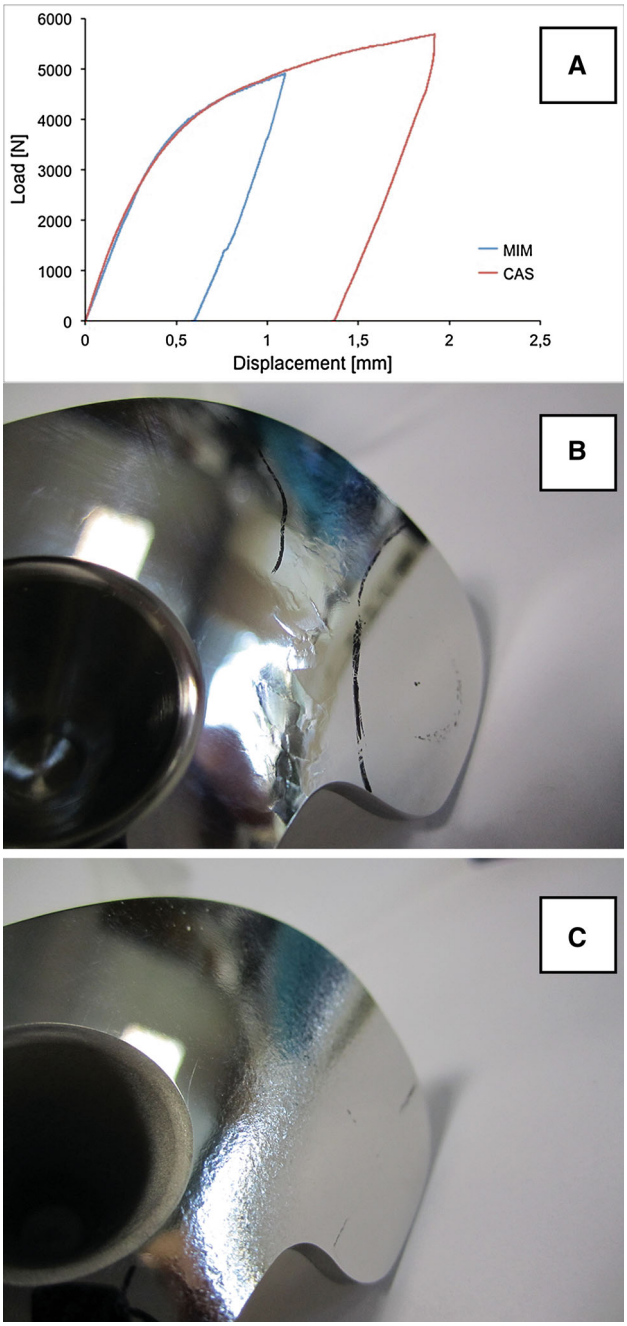

Fig. 8 a Static test of TT-MIM and TT-CAS in the configuration reported in Fig. 2a. **b** TT-CAS after test and **c** TT-MIM after test

amount of chromium carbide-based inclusions. On the other hand, similar Young moduli were obtained for both samples, as expected, since these are primarily determined by the alloy composition and do not depend much on microstructural features. Their values agree quite well with those available for hot isostatically pressed CoCrMo alloys in the literature [21, 22].

Scratch test results showed a better tribological behavior of the CAS sample. In fact, the higher hardness and the lower groove volume (V_G) in a single-asperity scratch contact suggest that abrasive grooves caused by hard counterbody asperities will be somewhat smaller. The higher V_P/V_G ratio also indicates that the material has larger near-surface plastic deformability and better resistance against abrasive wear by hard sliding counterparts. The V_P/V_G ratio is indeed directly related to the $\varepsilon_C/\varepsilon_S$ ratio between the threshold deformation for material removal (ε_C) and the actual surface deformation during grooving (ε_S), as well as to the strain hardening behavior of the material. Various analytical expressions have indeed been proposed by different authors, such as: $V_P/V_G = exp\left(-2\left(H_0/H\right)^{1/3}\ln\left(\varepsilon_S/\varepsilon_C\right)\right)$, where H_0 and H are the surface hardness values before and after plastic deformation [23], or $V_P/V_G = \left(\varepsilon_C/\varepsilon_S\right)^{2/\beta}$, where β is a quantity related to strain-hardening [24]. Since, in the present scratch experiments, the surface deformation ε_S is similar for both materials (though not identical, because of the slight difference in indenter penetration depth), the higher value of V_P/V_G for the CAS sample implies higher critical strain for material removal (ε_C) and, perhaps, a more marked strain-hardening behavior. Again, the higher ε_C of the CAS sample can be related to its finer grain structure and to the strengthening effect of the carbide precipitates.

It has accordingly been shown by the authors that metallic surfaces with higher V_P/V_G ratio tend to exhibit better resistance to abrasive grooving by hard counterparts in sliding contact, because such higher deformabilty (higher ε_C) promotes a tendency towards microploughing (with plastic displacement of material to the groove sides) rather than towards the more dangerous microcutting mechanism (with direct removal of an abrasion chip in front of the advancing asperity) [25, 26]. It is therefore analogously expected that, in sliding contact with hard, abrasive counterparts, the CAS sample will exhibit somewhat better wear resistance than the MIM one.

Dry wear tests performed under the lowest load of 3 N do confirm the slightly better tribological behavior of CAS samples over MIM ones. However, the situation is reversed at the highest load, with the appearance of small pits on the surface of the CAS samples, suggesting that fragmentation of the chromium carbide inclusions observed in [12] and their consequent pull-out from the surface may be occurring because of the excessively large contact pressure and of the lack of support from the softer surrounding metal matrix. Fracturing and pull-out of carbides weakens the sample surface and releases additional abrasive particles in the contact area, thus accounting for the increased wear rate of the cast sample at 5 N normal load.

Table 3 Stair case sequence on TT-MIM specimens

Order						Lmax	Lmin	Lamp	Lav
						3,115	311	1,402	1,713
	X		X			3,024	302	1,361	1,663
O		O		X		2,933	293	1,320	1,613
					O	2,842	284	1,279	1,563
						2,751	275	1,238	1,513
5,000,000	791,000	5,000,000	729,540	623,180	5,000,000	N° of cycles			

"X" indicates the broken ones while "O" indicates specimens which passed the 5 millions test. At the bottom of this table the number of cycles performed is reported. In the right columns Lmax, the maximum load, Lmin, the minimum, Lav, the medium value, and Lamp, the sinusoid amplitude, are reported (in N)

Table 4 Stair case sequence on TT-CAS specimens

Order						Lmax	Lmin	Lamp	Lav
						3,364	336	1,514	1,850
			X		O	3,273	327	1,473	1,800
X		O		O		3,182	318	1,423	1,750
	O					3,091	309	1,391	1,650
						3,000	300	1,350	1,600
1,664,242	5,000,000	5,000,000	535,198	5,000,000	5,000,000	N° of cycles			

"X" indicates the broken ones while "O" indicates specimens which passed the 5 Millions test. At the bottom of this table the number of cycles performed is reported. In the right columns Lmax, the maximum load, Lmin, the minimum, Lav, the medium value, and Lamp, the sinusoid amplitude, are reported (in N)

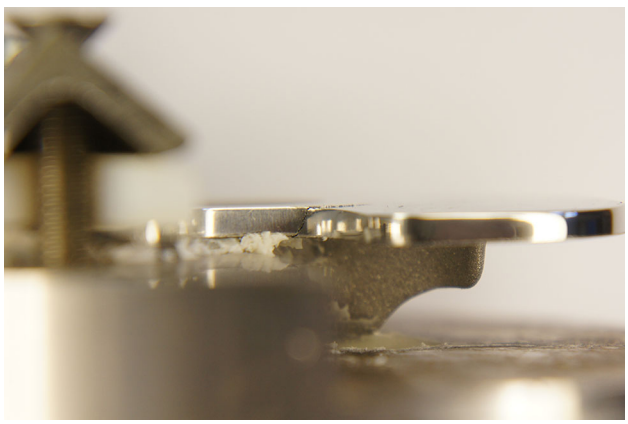

Fig. 9 Fatigue crack observed in the frontal plane

In wet wear test, the solution plays a lubricant role, reducing the contact pressure and therefore preventing carbide fracturing in the CAS sample (in spite of the 5 N normal load), so that the latter exhibits slightly better wear resistance than the MIM one, consistent with its higher hardness and higher V_P/V_G ratio (lower sensitivity to abrasive wear). Wear rate values obtained for both samples are, however, in substantial accordance with the reportedly good wear properties of CoCrMo alloys in prosthetic applications [27]. From the clinical point of view, some concerns could arise about the reduction of tribological properties of MIM CoCrMo, because of the major role that aseptic loosening has acquired in the past decade among causes of TKA failures. [28] Nevertheless, it has also been observed that there were no huge differences in the clinical and radiological midterm outcome of titanium alloy and polished CoCr tibial trays, in TKA. [29] Based on these facts MIM CoCrMo appears suitable for liquid-mediated sliding wear contacts against hard counterbodies. Moreover, the MIM sample would also reduce or eliminate the possibilities of a release of carbide fragments in case of accidental contact overloading, which might instead happen with CAS samples as demonstrated by dry sliding tribological tests under high normal load conditions.

4.2 Device fatigue performance

ISO and ASTM standards propose a screening test to evaluate the fatigue resistance of tibial trays. After Ahir studies [13, 14] and other studies of loading during daily activities at joint level [30], the threshold fatigue limit has been described, for a defined tibial tray design. The test was passed if five specimens, selected in the worst-case design condition, didn't show any failure sign after 5 millions cycles, following ISO 14879-1 directions, or 10 millions cycles, following ASTM F1800 ones. Paul

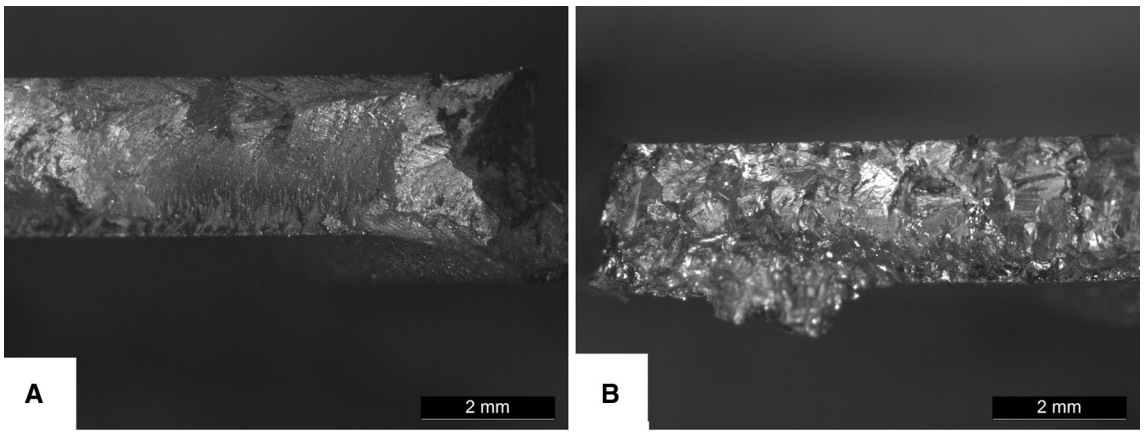

Fig. 10 Fracture surface of **a** TT-CAS and **b** TT-MIM, after fatigue failure

suggested that 10 millions cycles describe best the number of loading cycles foreseen in vivo [30].

Here we decided to evaluate the comparison between the two equal designed, CAS and MIM tibial trays, following ISO standard in the non-physiological loading condition of total rollback of the knee joint. Such load application point was selected because it induces the highest stresses in the tested device.

The fatigue limit observed, (1,625 $\pm$ 44) N for TT-MIM and (1,766 $\pm$ 52) N for TT-CAS, exceeds the threshold of 900 N of maximum loading suggested by the ISO standard; therefore, TT-MIM could be suitable for clinical application.

The difference in the fatigue limit, calculated through the Dixon's statistical approach, could be totally ascribed to the base material, which, as shown before [12], results in a different microstructure, due to manufacturing process. Especially the presence of a distributed porosity in the MIM material (as recalled in Sect. 4.1) might have some role in reducing the fatigue life, although the effect is not particularly deleterious because of the very fine pore size [12]. It should be pointed out that those values are not absolute and they apply only to the specific geometry and design of the TT tested.

The transgranular fracture observed in TT-MIM, (Fig. 10b) is actually coherent with the polygonal MIM grain structure, abundant of stacking fault defects [12]. Furthermore, a similar behavior has been observed along the boundaries of the sliding wear track on MIM specimens (Fig. 7b), where sliding lines, with different preferential orientations in different areas, seem to highlight the existence of preferential sliding planes in each of the crystalline grains, each having different orientation.

This fracture mechanism, that follows the weakest planes of the MIM microstructure, cannot be seen in the TT-CAS probably because of the more irregular, dendritic grain structure, in which the fine carbide dispersion could also have a crack deflection effect [12].

It should be noted however that the highest physiological load peaks are usually equivalent to 3.5 times the body weight for knee joint, and they are present in activities such as stair descending that doesn't involve the total rollback position, in which TT MIM and CAS have been tested [31]. Higher fatigue limits are thus expected for load conditions more similar to everyday knee loading and good outcome for TT MIM is again expected.

In order to better understand this phenomenology and obtain values useful for medical device designer, further fatigue tests on simple CoCrMo cast and MIM should be performed using a damage-tolerant approach. The great influence of post processes on CoCrMo alloy for biomedical applications has already been highlighted, showing an almost doubled fatigue limit for forged and hot isostatic pressed alloy compared to the cast one [32].

The next step should be the evaluation of the fatigue performance coupled with the wear in PBS environment, in order to better simulate the in vivo behavior of the new manufactured CoCrMo alloy. Eventually, tests performed in a knee simulator could highlight the tribo-mechanical performance of the new MIM device compared to the traditional one, obtaining results more relatable to the actual in vivo behavior.

5 Conclusions

The present paper investigated the mechanical properties of metal injection molded (MIM) CoCrMo alloys for implantable prosthetic devices, and the fatigue performance of MIM tibial trays, being MIM a lower cost alternative processing technology to conventional manufacturing routes such as investment casting.

From the micromechanical point of view, differences exist between CoCrMo alloys processed by MIM and by investment casting. Whereas the latter exhibited a Vickers hardness value of ≈ 514 HV_{3N}, MIM had shown a lower one of ≈ 335 HV_{3N}. In single-asperity scratch contacts, the MIM CoCrMo alloy accordingly develops larger grooves than the corresponding cast alloy, with higher tendency toward microcutting rather than microploughing. Its resistance against wear by sliding of hard counterparts is therefore somewhat lower than that of the cast alloy, unless contact pressures become large enough to cause fracturing and pull-out of carbides from the latter. Differences, however, are not very large; both MIM and cast alloys exhibit poor tribological behaviour in dry sliding but much better and satisfactory wear resistance when immersed in body fluid solution.

The final device fatigue resistance appeared statistically slightly lower in the case of MIM tibial trays compared to cast trays having the same design. This aspect is attributed to a more brittle behaviour of the MIM microstructure, as shown by the fracture surface morphologies. A toughening effect of the fine carbide dispersion, previously observed in the cast microstructure, has been hypothesized, although further analysis on the material fatigue behavior is needed.

In spite of that, all the MIM tibial trays showed a fatigue limit higher than the ISO and ASTM threshold value and therefore they are suitable for clinical application.

Acknowledgments Authors acknowledge SAMO and Regione Emilia Romagna for funding. The research was funded by Centro Interdipartimentale INTERMECH MO.RE. located at the Department of Engineering "Enzo Ferrari", University of Modena and Reggio Emilia, and by Regione Emilia Romagna, Italy. Thanks are due to Mr. Corrado Iotti for his contribution to the experimental activities.

Conflict of interest Research has been founded by Regione Emilia Romagna and conducted in cooperation with SAMO Biomedica, an Italian producer of implantable prostheses.

References

1. Dixon T, Shaw M, Ebrahim S, Dieppe P. Trends in hip and knee joint replacement: socioeconomic inequalities and projections of need. Ann Rheum Dis. 2004;63(7):825–30.
2. Kurtz S, Ong K, Lau E, Mowat F, Halpern M. Projections of primary and revision hip and knee arthroplasty in the United States from 2005 to 2030. J Bone Joint Surg. 2007;89(4):780–5.
3. Sonntag R, Reinders J, Kretzer JP. What's next? Alternative materials for articulation in total joint replacement. Acta Biomater. 2012;8(7):2434–41.
4. Barber TC, Healy WL. The hospital cost of total hip arthroplasty. J Bone Joint Surg Am. 1993;75(3):321–5.
5. Berry G, Bolton JD, Brown JB, McQuaide S (1999) Production and properties of wrought high carbon Co–Cr–Mo alloys. In Cobalt-Base Alloys for Biomedical Applications; Norfolk, VA:3-4 Nov 1998, pp. 11–31.
6. Dearnley PA. A review of metallic, ceramic and surface-treated metals used for bearing surfaces in human joint replacements. P I Mech Eng H. 1999;213(2):107–35.
7. Nasab MB, Hassan MR. Metallic biomaterials of knee and hip: a review. Trends Biomater Artificial Organs. 2010;24(1):69–82.
8. Tandon R. Net-shaping of Co-Cr-Mo(F-75) via metal injection molding. ASTM Spec Tech Publ. 1999;1365:3–10.
9. Muterlle PV, Zendron M, Zanella C, Perina M, Bardini R, Molinari A. Effect of Microstructure on the properties of a biomedical Co-Cr-Mo Alloy Produced by MIM. Proceedings of the 2009 International Conference on Powder Metallurgy & Particulate Materials, June 28–July 1, Las Vegas, Nevada 2009.
10. Muterlle PV, Lonardelli I, Perina M, Zendron M, Bardini R, Molinari A. Solution annealing and aging of a MIM CoCrMo alloy. Int J Powder Metall. 2010;46(4):43–51.
11. Muterlle PV, Zendron M, Perina M, Bardini R, Molinari A. Microstructure and tensile properties of metal injection molding Co–29Cr–6Mo–0.23C alloy. J Mater Sci. 2010;45:1091–9.
12. Melli V, Rondelli G, Sandrini E, Altomare L, Bolelli G, Bonferroni B, Lusvarghi L, De Nardo L. Metal injection molding as enabling technology for the production of metal prosthesis components: electrochemical and in vitro characterization. J Biomed Mater Res B. 2013;101(7):1294–301.
13. Ahir SP, Blunn GW, Haider J, Walker PS. Evaluation of a testing method for the fatigue performance of total knee tibial trays. J Biomech. 1999;32:1049–57.
14. Ahir SP, Blunn G, Harison M, Haider H, Walker PS. Pre-clinical testing of tibial tray designs for their fatigue performance. Combined Orthopaedic Researc Societies Meeting 2001.
15. Villa T, Migliavacca F, Gastaldi D, Colombo M, Pietrabissa R. Contact stresses and fatigue life in a knee prosthesis: comparison between in vitro measurements and computational simulations. J Biomech. 2004;37:45–53.
16. Yu T-C, Huang C-H, Hsieh C-H, Liau J-J, Huang C-H, Cheng C-K. Fatigue resistance analysis of tibial baseplate in total knee prosthesis: an in vitro biomechanical study. Clin Biomech. 2006;21:147–51.
17. Oliver WC, Pharr GM. An improved technique for determining hardness and elastic modulus using load and displacement sensing indentation experiments. J Mater Res. 1992;7(6):1564–83.
18. Kokubo T, Takadama H. How useful is SBF in predicting in vivo bone bioactivity? Biomaterials. 2006;27(15):2907–15.
19. Dixon WJ, Massey FJ. Introduction to statistical analysis. 4 (International student ed) ed. Auckland: McGraw Hill; 1983.
20. Ashby M, Abulawi J, et al. Temperature maps for frictional heating in dry sliding. Tribol T. 1991;34(4):577–87.
21. Brunski JB. Metals. In: Ratner BD, Hoffman AS, Schoen FJ, Lemons JE, editors. Biomaterials Science: An Introduction to Materials in Medicine. London: Elsevier Academic Press; 1996. p. 37–50.
22. Teoh SH. Introduction to biomaterials engineering and processing: an overview. In: Teoh SH, editor. Biomaterials engineering and processing Series Vol 1: engineering materials for biomedical applications. Singapore: World Scientific Publishing; 2004. p. 1–16.
23. Stachwiak GW, Batchelor AW. Engineering tribology. 3rd ed. Burlington: Elsevier; 2005. p. 507–8.
24. Kato K, Adachi K. Wear mechanisms. Modern tribology handbook. 2001;1:273–300.
25. Bolelli G, Cannillo V, et al. Microstructural and tribological comparison of HVOF-sprayed and post-treated M-Mo–Cr–Si (M = Co, Ni) alloy coatings. Wear. 2007;263(7–12):1397–416.
26. Bolelli G, Bonferroni B, et al. Micromechanical properties and sliding wear behaviour of HVOF-sprayed Fe-based alloy coatings. Wear. 2012;276–277:29–47.

27. Pilliar R. Metallic Biomaterials. In: Narayan R, editor. Biomedical materials. New York: Springer; 2009. p. 41–81.
28. Sharkey PF, Lichstein PM, et al. Why are total knee arthroplasties failing today: has anything changed after 10 years? J Arthroplasty. 2014. doi:10.1016/j.arth.2013.07.024.
29. Hug KT, Henderson RA, et al. Polished cobalt-chrome vs titanium tibial trays in total knee replacement (a comparison using the PFC Sigma system). Duke Orthop J. 2011;2(1):5–11.
30. Paul JP. Strenght requirements for internal and external prosthesis. J Biomech. 1999;32:381–93.
31. Kutzner I, Heinlein B, et al. Loading of the knee joint during activities of daily living measured in vivo in five subjects. J Biomech. 2010;43:2164–73.
32. Teoh SH. Fatigue of biomaterials: a review. Int J Fatigue. 2000;22:825–37.